Supplemental Material for "Transformations Based on Continuous Piecewise-Affine Velocity Fields"

Oren Freifeld, *Member, IEEE,* Søren Hauberg, *Member, IEEE,* Kayhan Batmanghelich, *Member, IEEE,* and Jonn W. Fisher III, *Member, IEEE,*

Abstract

In addition to the **attached two videos** (mentioned in the paper), this supplemental material contains:

1) Visualization of a CPA basis for a nominal type-II tessellation in 2D.
2) A deformation example: from a rectangular bar to a horseshoe.
3) Results for the timings experiments.
4) Proofs for the lemmas and theorems (except the proofs of the Lemma 2 and Theorem 2 that appear in the main text).

- *Oren Freifeld is with the Department of Computer Science, Ben-Gurion University, Be'er Sheva 84105 Israel. E-mail: orenfr@cs.bgu.ac.il*
- *K. Batmanghelich and J.W. Fisher III are with the Computer Science and Artificial Intelligence Lab, Massachusetts Institute of Technology, Cambridge MA 02319, USA. E-mail: {kayhan, Fisher}@csail.mit.edu*
- *S. Hauberg is with the Section for Cognitive Systems, DTU Compute, Kongens Lyngby, Denmark 2800. E-mail: sohau@dtu.dk*

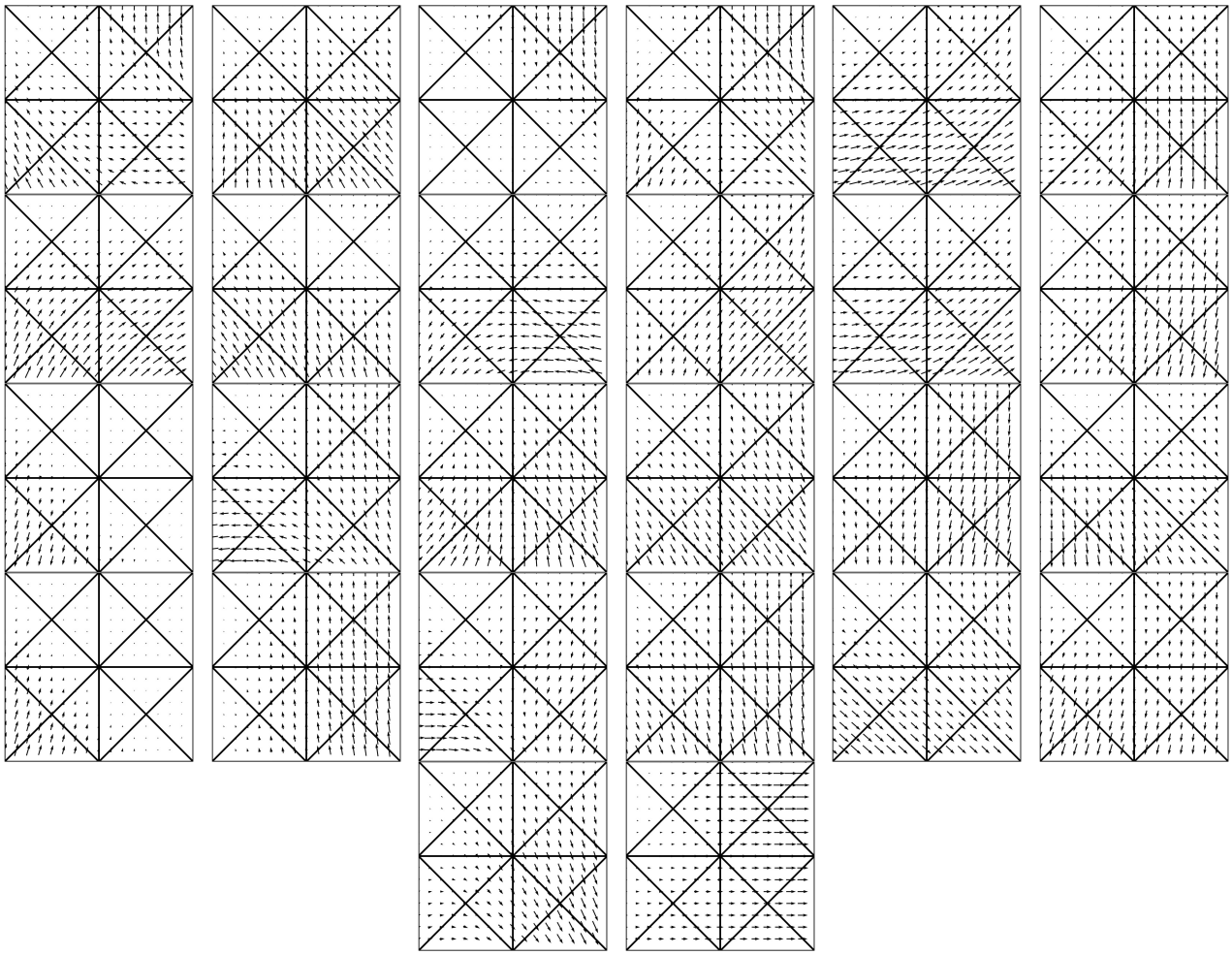

Fig. 1: The vector fields that constitute a 26-dimensional orthonormal basis of $\mathcal{V}$, obtained by SVD on B. The reason $d = 26$ is as follows. Note that the tessellation here is $\mathcal{P}_2$ (see Fig 3.b in the paper). Its associated dimension, $d = 26$, appears in Table 1 in the paper. More generally, this follows from Lemma 1: "...$d \triangleq \dim(\mathcal{V}) \leq nN_v$ with equality if and only if $\mathcal{P}$ is of type I". Here $n = 2$ (since we are in 2D) and there $N_v = 13$ vertices. Since this is a type-I tessellation, we have equality.

$N_{\mathcal{P}}$	5	25	45	65	85	105
our proposed solver	0.06	0.08	0.08	0.09	0.11	0.12
a generic solver	0.33	0.43	0.41	0.43	0.47	0.48

TABLE 1: Timing comparison (1D). Results, in [sec], are averages of timings of integration of random CPA fields. The tessellations, of $[0, 1]$, consist of $N_{\mathcal{P}}$ intervals of equal length. $N_{\text{pts}} = 10^5$, $N_{\text{steps}} = 100$ and $n_{\text{steps}} = 10$ (see Algorithm 1).

1 Visualization of a CPA Basis in the 2D Case

Figure 1 depicts the CPA fields that form a basis for $\mathcal{V}$ (a 2D case and a nominal type-I tessellation).

2 A Deformation Example: From a Rectangular Bar to a Horseshoe

The example in Fig. 2 shows a CPA velocity fields that leads to a CPAB transformation that deforms a rectangular bar to a Horseshoe-like shape.

3 Results for the Timings Experiments

We timed our GPU implementations (of both Algorithm 1 and the generic solver) on an Nvidia GTX 780 card. Table 1 (1D), Table 2 (2D, type-I cells) and Table 3 (2D, type-II cells) compare the specialized solver and a generic one on different tessellations. These comparisons show an overall clear win of the proposed solver. An only exception is $\mathcal{P}_v$ in Table 3, caused by the fact that in this resolution the boundaries were crossed too often, rendering Algorithm 1 almost equals to the generic solver, *except* that it also pays the overhead of boundary-crossing checks and computing $N_{\mathcal{P}}$ matrix exponentials. We expect that eventually, as $N_{\mathcal{P}}$ grows too large, this will also happen for type-I tessellations but memory limitations prevent us from verifying it (note also that this issue arises only for a very large $N_{\mathcal{P}}$ where d is so large that inference is

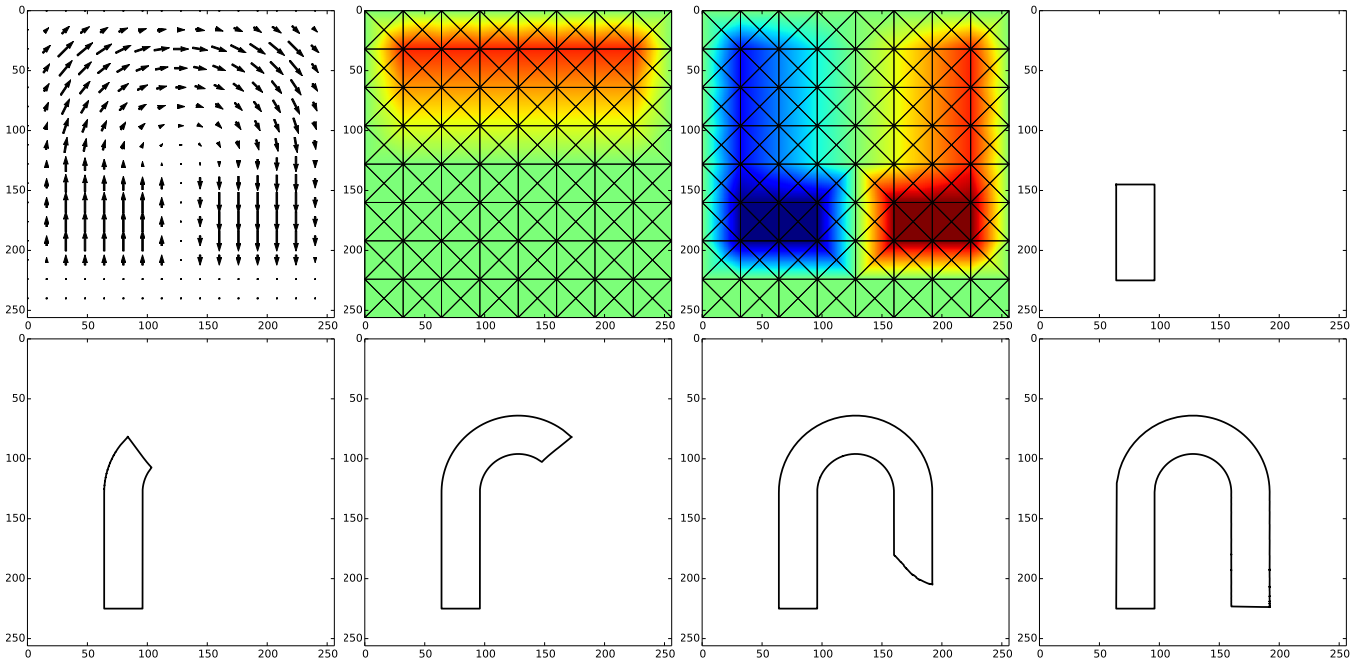

Fig. 2: Top left to bottom right: $\boldsymbol{v}^{\boldsymbol{\theta}}$, its horizontal and vertical components, and 5 steps of a rectangle-to-horseshoe process. The lower bar of the rectangle does not move since $\boldsymbol{v}^{\boldsymbol{\theta}} = 0$ in this location, while the upper bar eventually stops when the horseshoe is completed (for the same reason).

$\mathcal{P}$	$\mathcal{P}_1$	$\mathcal{P}_2$	$\mathcal{P}_3$	$\mathcal{P}_4$	$\mathcal{P}_5$
our proposed solver	0.06	0.09	0.15	0.24	0.27
a generic solver	0.22	0.23	0.25	0.26	0.28

TABLE 2: Timing comparison (2D, type-I cells). Results, in [sec], are averages of timings of integration of random CPA fields. The tessellations are as in Fig. 3 from the paper, the image size is 512×512, $N_{\text{steps}} = 100$ and $n_{\text{steps}} = 10$ (see Algorithm 1).

hard anyway). We thus suggest, for an overly-fine $\mathcal{P}$, to verify empirically which solver is faster (the answer also depends on the graphics card).

Table 4 shows how N_{steps} and N_{pts} affect the timings. Empirically, $N_{\text{steps}} = 10$ typically sufficed for good results.

4 Proofs

In what follows, the operations of multiplication of a map by a scalar and addition of two maps are defined in the standard way; *i.e.*, if f and g are two $\Omega \to \mathbb{R}^n$ maps and $\alpha \in \mathbb{R}$, we define

$$(f+g) : \boldsymbol{x} \mapsto f(\boldsymbol{x}) + g(\boldsymbol{x}) \quad \text{and} \quad (\alpha f) : \boldsymbol{x} \mapsto \alpha f(\boldsymbol{x})\,. \tag{1}$$

$\mathcal{P}$	$\mathcal{P}_i$	$\mathcal{P}_{ii}$	$\mathcal{P}_{iii}$	$\mathcal{P}_{iv}$	$\mathcal{P}_v$
our proposed solver	0.004	0.006	0.009	0.014	0.025
a generic solver	0.021	0.020	0.019	0.021	0.023

TABLE 3: Timing comparison (2D, type-II cells). The setting is as in Table 2 except the tessellations which are from Fig. 4 from the paper.

N_{pts}	N_{steps}	$\mathcal{P}_1$	$\mathcal{P}_2$	$\mathcal{P}_3$	$\mathcal{P}_4$	$\mathcal{P}_5$
64×64	10	.001	.001	.002	.002	.006
64×64	100	.002	.003	.003	.005	.014
256×256	10	.004	.006	.009	.011	.014
256×256	100	.023	.028	.046	.064	.083
512×512	10	.011	.016	.025	.036	.041
512×512	100	.079	.129	.185	.287	.300
1024×1024	10	.031	.051	.083	.146	.143
1024×1024	100	.255	.414	.519	1.005	1.070

TABLE 4: Timings (in [sec]) for varying N_{pts} and N_{steps}. The setup is as the one described in in Table 2.

Proof of Lemma 1. **First**, we prove $\mathcal{V}'$ is linear by showing its closure under linear combinations. Let $\alpha \in \mathbb{R}$ and let f and f' be two PA maps, where $f : \boldsymbol{x} \mapsto A_{\gamma(\boldsymbol{x})}\widetilde{\boldsymbol{x}}$ and $f' : \boldsymbol{x} \mapsto A'_{\gamma(\boldsymbol{x})}\widetilde{\boldsymbol{x}}$. Now note that $\alpha f : \boldsymbol{x} \mapsto \alpha \left(A_{\gamma(\boldsymbol{x})}\widetilde{\boldsymbol{x}}\right) = \left(\alpha A_{\gamma(\boldsymbol{x})}\right)\widetilde{\boldsymbol{x}}$ and $f + f' : \boldsymbol{x} \mapsto A_{\gamma(\boldsymbol{x})}\widetilde{\boldsymbol{x}} + A'_{\gamma(\boldsymbol{x})}\widetilde{\boldsymbol{x}} = \left(A_{\gamma(\boldsymbol{x})} + A'_{\gamma(\boldsymbol{x})}\right)\widetilde{\boldsymbol{x}}$ are PA maps, as follows from the linearity of $\mathbb{R}^{n\times(n+1)}$. **Second**, since $\mathcal{V}$ is the intersection of two linear spaces, $\mathcal{V}$ and the space of $\Omega \to \mathbb{R}^n$ continuous maps, it follows that $\mathcal{V}$ is a linear space too. **Third**, that $D \triangleq \dim(\mathcal{V}) = (n^2+n) \times N_{\mathcal{P}}$ is trivial since any element of $\mathcal{V}'$ is defined by $N_{\mathcal{P}}$ (unconstrained) matrices of size $n \times (n+1)$. **Fourth**, assume $\mathcal{P}$ is a type-I tessellation. It follows that the values a CPA map takes at the vertices in a given cell uniquely define the A of that cell (and as we will see in the proof of Lemma 2, continuity of the field across inter-cell boundaries follows from the continuity at the vertices). Since in each one of these N_v vertices there are n degrees of freedom, it follows that $d \triangleq \dim(\mathcal{V}) = n \times N_v$. **Finally**, let $\mathcal{P}'$ be a tessellation that contains a cell which is not of type I. Then we can always partition this cell into type-I cells by simply adding vertices. In other words, for every non-type-I tessellation, $\mathcal{P}'$, there exists a type-I tessellation, $\mathcal{P}$ which is a refinement of $\mathcal{P}'$. Note that $\dim(\mathcal{V}_{\Omega,\mathcal{P}'}) < \dim(\mathcal{V}_{\Omega,\mathcal{P}})$. Let ${N_v}'$ stands for the number of vertices in $\mathcal{P}'$. Note that ${N_v}' < N_v$. It follows that $\dim(\mathcal{V}_{\Omega,\mathcal{P}}) < D$. □

Recall that the columns of $\boldsymbol{B} = [\,\boldsymbol{B}_1 \,\cdots\, \boldsymbol{B}_d\,] \in \mathbb{R}^{D\times d}$ denote the orthonormal basis of $\mathrm{null}(L)$ obtained via SVD.

Proof of Lemma 3. The matrix associated with $L_{\boldsymbol{v}^{\boldsymbol{\theta}}_{\mathrm{vert}} \mapsto \boldsymbol{\theta}}$ is a transition matrix between two known $d-$dimensional bases. □

Example 1. For concreteness, let us look at a type-I tessellation when $n = 2$, the other cases being essentially identical. Let $\boldsymbol{x}_1$, $\boldsymbol{x}_2$ and $\boldsymbol{x}_3$ denote the vertices of a (non-degenerate) triangle, and let $\boldsymbol{v}_1$, $\boldsymbol{v}_2$ and $\boldsymbol{v}_3$ denote the values a CPA velocity field takes at these vertices, respectively. Letting $A = \left[\begin{smallmatrix} a_{11} & a_{12} & a_{13} \\ a_{21} & a_{22} & a_{23} \end{smallmatrix}\right]$ denote the matrix associated with this triangle, we have

$$\underset{6\times 1}{\begin{bmatrix} \boldsymbol{v}_1 \\ \boldsymbol{v}_2 \\ \boldsymbol{v}_3 \end{bmatrix}} = \underset{6\times 1}{\begin{bmatrix} A\widetilde{\boldsymbol{x}}_1 \\ A\widetilde{\boldsymbol{x}}_2 \\ A\widetilde{\boldsymbol{x}}_3 \end{bmatrix}} = \underset{6\times 6}{\begin{bmatrix} \widetilde{\boldsymbol{x}}_1^T & \boldsymbol{0}_{1\times 3} \\ \boldsymbol{0}_{1\times 3} & \widetilde{\boldsymbol{x}}_1^T \\ \widetilde{\boldsymbol{x}}_2^T & \boldsymbol{0}_{1\times 3} \\ \boldsymbol{0}_{1\times 3} & \widetilde{\boldsymbol{x}}_3^T \\ \widetilde{\boldsymbol{x}}_3^T & \boldsymbol{0}_{1\times 3} \\ \boldsymbol{0}_{1\times 3} & \widetilde{\boldsymbol{x}}_3^T \end{bmatrix}} \begin{bmatrix} a_{11} \\ a_{12} \\ a_{13} \\ a_{21} \\ a_{22} \\ a_{23} \end{bmatrix} \Longrightarrow \begin{bmatrix} a_{11} \\ a_{12} \\ a_{13} \\ a_{21} \\ a_{22} \\ a_{23} \end{bmatrix} = \begin{bmatrix} \boldsymbol{v}_1 \\ \boldsymbol{v}_2 \\ \boldsymbol{v}_3 \end{bmatrix} \begin{bmatrix} \widetilde{\boldsymbol{x}}_1^T & \boldsymbol{0}_{1\times 3} \\ \boldsymbol{0}_{1\times 3} & \widetilde{\boldsymbol{x}}_1^T \\ \widetilde{\boldsymbol{x}}_2^T & \boldsymbol{0}_{1\times 3} \\ \boldsymbol{0}_{1\times 3} & \widetilde{\boldsymbol{x}}_3^T \\ \widetilde{\boldsymbol{x}}_3^T & \boldsymbol{0}_{1\times 3} \\ \boldsymbol{0}_{1\times 3} & \widetilde{\boldsymbol{x}}_3^T \end{bmatrix}^{-1} \tag{2}$$

(end of the example).

Proof of Lemma 4. We again focus on the case where $n = 2$, the other cases being similar. To enforce zero traces, we add to L rows derived from the following constraints:

$$\begin{bmatrix} 1 & 0 & 0 & 0 & 1 & 0 \end{bmatrix} \mathrm{vec}(A_c) = 0 \qquad\qquad \forall\, c \in \{1, \ldots, N_{\mathcal{P}}\}\,. \tag{3}$$

Likewise, to nullify, *e.g.*, the horizontal component of the velocity across the rightmost boundary of $\Omega = [0, x_{\max}] \times [0, y_{\max}]$ we add rows derived from the constraints

$$\begin{bmatrix} \widetilde{\boldsymbol{x}}_a^T & \boldsymbol{0}_{1\times 3} \end{bmatrix} \mathrm{vec}(A_c) = 0 \tag{4}$$

for every vertex $\boldsymbol{x}_a$ of some cell U_c such that $\boldsymbol{x}$ is on the rightmost boundary of Ω. □

Proof of Lemma 5. In case $n = 1$ and $\Omega = [x_{\mathrm{xmin}}, x_{\mathrm{xmax}}]$, we extend the leftmost and rightmost intervals to $-\infty$ and ∞, respectively, with adding no cells or constraints on $\boldsymbol{v}^{\boldsymbol{\theta}}$. If $n > 1$ and the tessellation is a regular one of type II (*i.e.*, the cells are hyperrectangles) the extension is trivial and be made by (non-compact) hyperrectnalges. Now consider type-I tessellations for $n \geq 2$. If $n = 2$ and Ω is a rectangle, we extend the outer cells of $\mathcal{P}$ (rendering them non-triangular) to cover the whole of $\mathbb{R}^2$ and add certain additional continuity constrains on $\boldsymbol{v}^{\theta}$. The process is best explained by Fig. 3. By an argument similar to the one used earlier to describe how continuity at two points ensures continuity of a PA field on their join, this process ensures the extended field is CPA over the whole of $\mathbb{R}^2$. Mathematically, the case with $n = 3$ can be handled in a similar-but-more-tedious way. However, unlike all the other 3D-related options mentioned in the paper, we did not implement this option for the 3D case. Rather, we opted to ensure the CPA property by imposing zero-boundary constraints. For $n > 3$, the general case is hard to implement, but, at least conceptually, can be done in a similar way to the above. However, we remind the reader that we stated in the paper that for $n > 3$ we use only type-II tessellations. □

Before proceeding to the proof of the theorem, recall that the solution, $t \mapsto \psi^t_{\boldsymbol{\theta},c}(\boldsymbol{x})$, to an ODE with an $\Omega \to \mathbb{R}^n$ *affine* velocity field, $\boldsymbol{x} \mapsto A_{c,\boldsymbol{\theta}}\widetilde{\boldsymbol{x}}$, is

$$\begin{bmatrix} \psi^t_{\boldsymbol{\theta},c}(\boldsymbol{x}) \\ 1 \end{bmatrix} \triangleq T_{A_{c,\boldsymbol{\theta}},t}\widetilde{\boldsymbol{x}}\,, \qquad A_{c,\boldsymbol{\theta}} \in \mathbb{R}^{n\times(n+1)}\,, \qquad T_{A_{c,\boldsymbol{\theta}},t} \triangleq \mathbf{expm}(t\widetilde{A_{c,\boldsymbol{\theta}}})\,, \qquad \widetilde{A_{c,\boldsymbol{\theta}}} = \begin{bmatrix} A_{c,\boldsymbol{\theta}} \\ \boldsymbol{0}_{1\times n+1} \end{bmatrix}. \tag{5}$$

Also recall that $\boldsymbol{\phi}^{\boldsymbol{\theta}}(\boldsymbol{x}, t)$ is given by the concatenation of such solutions

$$\boxed{\boldsymbol{\phi}^{\boldsymbol{\theta}}(\boldsymbol{x}, t) = (\psi^{t_m}_{\boldsymbol{\theta},c_m} \circ \ldots \circ \psi^{t_2}_{\boldsymbol{\theta},c_2} \circ \psi^{t_1}_{\boldsymbol{\theta},c_1})(\boldsymbol{x})}\,, \tag{6}$$

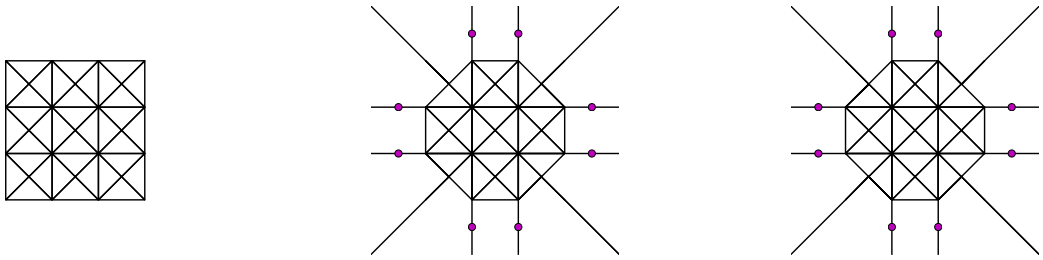

Fig. 3: Left: a triangular tessellation on compact region (a square in this case). Middle: Extending it to the whole of $\mathbb{R}^2$. The circles stand for auxiliary vertices where continuity is enforced (in addition to the continuity constraints at the original vertices, including the corners of the square). Right: Using the color scheme from the paper, and the extended tessellation, we show the horizontal component of some velocity field which is CPA on the whole of $\mathbb{R}^2$ (due to the additional constraints).

that $\exp(\boldsymbol{v}^\theta) \triangleq T^{\boldsymbol{\theta}}$ is defined via $T^{\boldsymbol{\theta}}(\boldsymbol{x}) = \boldsymbol{\phi}^{\boldsymbol{\theta}}(\boldsymbol{x}, 1)$, and that the compact notation in the boxed equation above hides an important detail: the number of the trajectory segments, their durations, and the cells involved (where a cell may appear more than once), *all depend on* $\boldsymbol{x}$. They all also depend on $\boldsymbol{\theta}$ and t, except the first cell; *i.e.*, $c_1 = \gamma(\boldsymbol{x})$; *i.e.*,

$$\boldsymbol{\phi}^{\boldsymbol{\theta}}(\boldsymbol{x}, t) = (\psi^{t_{m_{\boldsymbol{x},\boldsymbol{\theta},t}}(\boldsymbol{x},\boldsymbol{\theta},t)}_{\boldsymbol{\theta},c_{m_{\boldsymbol{x},\boldsymbol{\theta},t}}(\boldsymbol{x},\boldsymbol{\theta})} \circ \ldots \circ \psi^{t_2(\boldsymbol{x},\boldsymbol{\theta},t)}_{\boldsymbol{\theta},c_2(\boldsymbol{x},\boldsymbol{\theta})} \circ \psi^{t_1(\boldsymbol{x},\boldsymbol{\theta},t)}_{\boldsymbol{\theta},\gamma(\boldsymbol{x})})(\boldsymbol{x})\,. \tag{7}$$

Proof of Theorem 1. **Part (i).** For a given $\boldsymbol{x}$, the map $\boldsymbol{\theta} \mapsto \boldsymbol{v}^{\boldsymbol{\theta}}(\boldsymbol{x})$ is linear. Thus, $\boldsymbol{v}^{\boldsymbol{\theta}} = \boldsymbol{v}^{\alpha\boldsymbol{\theta}}/\alpha$. Moreover,

$$\xi^{\boldsymbol{\theta}}(\boldsymbol{x}, t) \triangleq \boldsymbol{\phi}^{\alpha\boldsymbol{\theta}}(\boldsymbol{x}, t/\alpha) = \boldsymbol{x} + \int_0^{t/\alpha} \boldsymbol{v}^{\alpha\boldsymbol{\theta}}(\boldsymbol{\phi}^{\alpha\boldsymbol{\theta}}(\boldsymbol{x}, \tau))\, d\tau = \boldsymbol{x} + \int_0^{t/\alpha} \alpha \boldsymbol{v}^{\boldsymbol{\theta}}(\boldsymbol{\phi}^{\alpha\boldsymbol{\theta}}(\boldsymbol{x}, \tau))\, d\tau \tag{8}$$

$$= \boldsymbol{x} + \int_0^{t} \boldsymbol{v}^{\boldsymbol{\theta}}(\boldsymbol{\phi}^{\alpha\boldsymbol{\theta}}(\boldsymbol{x}, \eta/\alpha))\, d\eta = \boldsymbol{x} + \int_0^{t} \boldsymbol{v}^{\boldsymbol{\theta}}(\xi^{\boldsymbol{\theta}}(\boldsymbol{x}, \eta))\, d\eta \tag{9}$$

and now observe that $\xi^{\boldsymbol{\theta}}(\cdot, t)$ coincides with $\boldsymbol{\phi}^{\boldsymbol{\theta}}(\cdot, t)$.

Part (ii). By applying the Picard-Lindelof theorem, and then extending the solution (to a finite t) we conclude that the trajectories do not intersect. From this it follows that $T^{\boldsymbol{\theta}}$ is invertible. Since $\boldsymbol{\theta} \mapsto \boldsymbol{v}^{\boldsymbol{\theta}}$ is linear, and since both $\mathbb{R}^d$ and $\mathcal{V}$ are linear spaces, we know that $\boldsymbol{v}^{-\boldsymbol{\theta}} \in \mathcal{V}$. Thus, by the definition of CPAB transformations, $T^{-\boldsymbol{\theta}} \in M$. We still, however, need to show that $T^{-\boldsymbol{\theta}} = (T^{\boldsymbol{\theta}})^{-1}$; *i.e.*, that $T^{-\boldsymbol{\theta}}$ is indeed the inverse of $T^{\boldsymbol{\theta}}$. By Eqn. (2) from the paper,

$$\boldsymbol{\phi}^{-\boldsymbol{\theta}}(\boldsymbol{\phi}^{\boldsymbol{\theta}}(\boldsymbol{x}, t), t) = \boldsymbol{\phi}^{\boldsymbol{\theta}}(\boldsymbol{x}, t) + \int_0^t \boldsymbol{v}^{-\boldsymbol{\theta}}(\boldsymbol{\phi}^{\boldsymbol{\theta}}(\boldsymbol{x}, \tau))\, d\tau = \boldsymbol{\phi}^{\boldsymbol{\theta}}(\boldsymbol{x}, t) - \int_0^t \boldsymbol{v}^{\boldsymbol{\theta}}(\boldsymbol{\phi}^{\boldsymbol{\theta}}(\boldsymbol{x}, \tau))\, d\tau = \boldsymbol{x} \tag{10}$$

where we used the fact the map $\boldsymbol{\theta} \mapsto \boldsymbol{v}^{\boldsymbol{\theta}}$ is linear (so $\boldsymbol{v}^{-\boldsymbol{\theta}} = -\boldsymbol{v}^{\boldsymbol{\theta}}$).

Part (iii). Since we showed that $(T^{\boldsymbol{\theta}})^{-1} = T^{-\boldsymbol{\theta}}$ and that $T^{-\boldsymbol{\theta}} \in M$, it is enough to show that any $T^{\boldsymbol{\theta}} \in M$ is differentiable. This is a known result for transformations obtained by integration of (stationary) Lipschitz-continuous velocity fields, but the CPA structure enables us to outline another proof, specialized to this case. Since $\boldsymbol{v}^{\boldsymbol{\theta}}$ is continuous, it follows that $\{t_i(\boldsymbol{x}, \boldsymbol{\theta}, t)\}_{i=1}^{m_{\boldsymbol{x},\boldsymbol{\theta},t}}$ are continuous functions of $\boldsymbol{x}$. The fact that $m_{\boldsymbol{x},\boldsymbol{\theta},t}$ changes with $\boldsymbol{x}$ does not change it. It just means a nominal t_i decreases continuously to zero or increases continuously from zero. Thus, taking the derivative of $\boldsymbol{\phi}^{\boldsymbol{\theta}}(\boldsymbol{x}, t)$ w.r.t. $\boldsymbol{x}$ results in summing terms of the form (notationally suppressing the dependency in t)

$$T_{\text{left},1}\, \frac{d\, \mathbf{expm}(\widetilde{t_i A_{c_i(\boldsymbol{x},\boldsymbol{\theta}),\boldsymbol{\theta}}})}{d\boldsymbol{x}}\, T_{\text{right},1} \; + T_{\text{left},2}\, \mathbf{expm}(\widetilde{t_i A_{c_i(\boldsymbol{x},\boldsymbol{\theta}),\boldsymbol{\theta}}})\, T_{\text{right},2} \tag{11}$$

where $T_{\text{left},1}$, $T_{\text{left},2}$, $T_{\text{right},1}$ and $T_{\text{right},2}$ are $(n+1) \times (n+1)$ matrices that change continuously with $\boldsymbol{x}$ (and also depend on i and $\boldsymbol{\theta}$). Likewise, the matrix $\widetilde{t_i A_{c_i(\boldsymbol{x},\boldsymbol{\theta}),\boldsymbol{\theta}}}$ changes continuously with $\boldsymbol{x}$. Thus, $\frac{d\, \mathbf{expm}(\widetilde{t_i A_{c_i(\boldsymbol{x},\boldsymbol{\theta}),\boldsymbol{\theta}}})}{d\boldsymbol{x}}$ is continuous too.

Part (iv). A well-known result is that in the case of an affine velocity field, $\boldsymbol{x} \mapsto A\widetilde{\boldsymbol{x}}$, a zero-trace A implies that, for any (finite) t, the resulting transformation,

$$\boldsymbol{x} \mapsto \begin{bmatrix} I_{n\times n} & \mathbf{0}_{n\times 1} \end{bmatrix} \mathbf{expm}(t\widetilde{A})\widetilde{\boldsymbol{x}}\,, \tag{12}$$

is volume preserving. From a Lagrangian standpoint, one way to show this is by noting that the determinant of the Jacobian matrix is one (since it is equal to the determinant of $\mathbf{expm}(t\widetilde{A})$ which is one since the trace is zero – a known property of $\mathbf{expm}$). From an Eulerian standpoint, this can be shown by applying the Divergence Theorem since a zero trace of A implies that the velocity field has zero divergence, and thus, by the Divergence theorem, no mass leaves or enters the region of interest (subject to a regularity condition on the boundary of the region). In the CPA case, if all the A's have zero

trace, then it can be similarly shown that the determinant of the Jacobian is still one (also verified numerically). However, it is easier to prove this using the Eulerian approach. Any region (whose boundary satisfies the regularity condition of the Divergence theorem) can be divided to smaller subregions such that each subregion is fully contained within some cell. In each such cell, the divergence of the field is zero and the Divergence theorem is applicable and thus the net inward flux (of mass, but by taking the density to be 1, it means volume) equals the net outward flux. Since the total flux is zero in every cell, the same holds for the entire region and we conclude the transformation is volume preserving. While this proof is restricted to regions whose boundary is regular, one can appeal to continuity arguments (approximating any non-regular boundary from inside and outside using regular boundaries) to prove the more general case.

Part (v). Any space whose elements are invertible $\Omega \to \Omega$ maps is nonlinear (w.r.t. the standard operations defined in Eqn. (1)), even if the maps themselves are linear[1]. To see that, note that the (constant) map, $\boldsymbol{x} \mapsto \mathbf{0}$, is the zero element of the linear space of all $\Omega \to \Omega$ maps (which contains M). This map is not invertible and is thus not in M. It follows that M is nonlinear since a linear subspace must contain the zero element of the larger linear space. As for the dimension, intuitively this follows from the fact that M is defined via the d-dimensional $\mathcal{V}$. We omit the formal proof (which is based on using $\exp$ to create a chart) as this is a standard result in differential geometry.

Part (vi). Since $\exp$ is smooth (particularity, it is uniformly continuous), it is enough to prove that $\mathcal{V}_{\Omega,\mathcal{P}_k}$ is dense in $C_\Omega^{\text{unif.}}$, the space of all uniformly-continuous velocity fields on Ω. Let $\boldsymbol{v} \in C_\Omega^{\text{unif.}}$. For every $k > 0$, there exists $\delta_k > 0$ such that $\|\boldsymbol{x} - \boldsymbol{y}\| < \delta_k \Rightarrow \|\boldsymbol{v}(\boldsymbol{x}) - \boldsymbol{v}(\boldsymbol{y})\| < \frac{1}{k}$. Let $\mathcal{P}_1$ to be some tessellation (of Ω) such that each cell can be bounded within a ball of radius 1. For $k > 1$, define $\mathcal{P}_k$ to be some tessellation that is a refinement of $\mathcal{P}_{k-1}$ and that each of its cells cab be bounded within a ball of radius $\frac{1}{2k}$. Thus, for a fixed k, within each cell, $\|\boldsymbol{v}(\boldsymbol{x}) - \boldsymbol{v}(\boldsymbol{y})\| < \frac{1}{2k}$. For $k \geq 1$, let $\boldsymbol{v}_k \in \mathcal{V}_{\Omega,\mathcal{P}_k}$ coincide with $\boldsymbol{v}$ on the vertices of $\mathcal{P}_k$. Thus, for a fixed k, within each cell, $\|\boldsymbol{v}_k(\boldsymbol{x}) - \boldsymbol{v}_k(\boldsymbol{y})\| < \frac{1}{2k}$ (since $\boldsymbol{v}_k$ is affine within the cell). By the triangle inequality, within each cell, $\|\boldsymbol{v}_k(\boldsymbol{x}) - \boldsymbol{v}(\boldsymbol{y})\| < \frac{1}{k}$. Letting k tend to ∞, we conclude that $\boldsymbol{v}_k$ converges to $\boldsymbol{v}$ uniformly. Thus, $\mathcal{V}_{\Omega,\mathcal{P}_k}$ is dense in $C_\Omega^{\text{unif.}}$. □

Finally, we remark that in the proof of Theorem 2 (which now appears in the main text) we customized the closed-form expression of a general 2-by-2 matrix exponential from [1] to the case where the second row is $[0, 0]$.

REFERENCES

[1] D. S. Bernstein and W. So, "Some explicit formulas for the matrix exponential," *Automatic Control, IEEE Transactions on*, vol. 38, no. 8, pp. 1228–1232, 1993.

1. *E.g.*, rotations in 3D are linear maps but $SO(3)$ is nonlinear.